NANO LETTERS

Letter

Graphene-Based Single-Bacterium Resolution Biodevice and DNA Transistor: Interfacing Graphene Derivatives with Nanoscale and Microscale Biocomponents

Nihar Mohanty, and Vikas Berry

Nano Lett., **2008**, 8 (12), 4469-4476 • Publication Date (Web): 05 November 2008

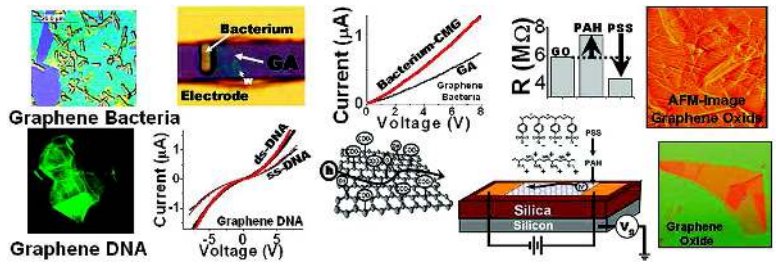

More About This Article

Additional resources and features associated with this article are available within the HTML version:

- Supporting Information
- Access to high resolution figures
- Links to articles and content related to this article
- Copyright permission to reproduce figures and/or text from this article

View the Full Text HTML

Nano Letters is published by the American Chemical Society. 1155 Sixteenth Street N.W., Washington, DC 20036

NANO LETTERS

2008
Vol. 8, No. 12
4469-4476

Graphene-Based Single-Bacterium Resolution Biodevice and DNA Transistor: Interfacing Graphene Derivatives with Nanoscale and Microscale Biocomponents

Nihar Mohanty and Vikas Berry*

Chemical Engineering, Kansas State University, Manhattan, Kansas 66506

Received August 8, 2008; Revised Manuscript Received October 3, 2008

ABSTRACT

Establishing "large-contact-area" interfaces of sensitive nanostructures with microbes and mammalian cells will lead to the development of valuable tools and devices for biodiagnostics and biomedicine. Chemically modified graphene (CMG) nanostructures with their microscale area, sensitive electrical properties, and modifiable chemical functionality are excellent candidates for such biodevices at both biocellular and biomolecular scale. Here, we report on the fabrication and functioning of a novel CMG-based (i) single-bacterium biodevice, (ii) label-free DNA sensor, and (iii) bacterial DNA/protein and polyelectrolyte chemical transistor. The bacteria biodevice was highly sensitive with a single-bacterium attachment generating ~1400 charge carriers in a p-type CMG. Similarly, single-stranded DNA tethered on graphene hybridizes with its complementary DNA strand to reversibly increase the hole density by 5.61×10^{12} cm^{-2}. We further demonstrate (a) a control on the device sensitivity by manipulating surface groups, (b) switching of polarity specificity by changing surface polarity, and (c) a preferential attachment of DNA on thicker CMG surfaces and sharp CMG wrinkles.

In the past decade, there have been a plethora of studies on building nano/bio interfaces with electrically, optically and thermally active nanoscale materials, which have tremendously advanced the fields of biomedicine,[1] bioactuated devices,[2,3] biodetection,[4−6] and diagnostics.[7,8] The current generation of electrically active nano/bio devices built using zero-dimensional (0D) nanoparticles,[8,9] one-dimensional (1D) nanowires,[4,10,11] and two-dimensional networks[12] have shown excellent detection and interfacing ability for both molecular (DNA, ATP, proteins, etc.) and nanoscale (viruses etc.) biocomponents. However, the incompatibility in areal dimensions makes it challenging to apply individual 0D and 1D nanostructures for building strong interfaces with larger-sized microorganisms or for retaining them on their networks.[12] Chemically modified graphenes (CMGs), with their two-dimensional nanostructures and adjustable surface chemistry, can interface strongly with the biological systems without geometric restrictions and without compromising the integrity of the microbial attachment.

Recently, chemical[13−17] and geometric[15,18−20] manipulation of graphene has shown great potential to control its band gap between semimetallic and semiconducting. Furthermore, with its low electrical noise (and low charge-scattering)[21−23] and ballistic transport,[22,24] graphene nanostructures have been incorporated into various electronic and optoelectronic applications[25] such as gas sensor,[26] transistors,[27,28] solar cells,[29−32] and liquid-crystal elements.[33] However, there has been no report on application of graphene in biological devices. Here, we demonstrate the interfacing of CMGs with biological systems to build a novel live-bacterial-hybrid device and a DNA-hybridization device with excellent sensitivity. We illustrate two crucial characteristics of the CMGs which make them promising building blocks for biodevices. First, via chemical modification and subsequent integration of CMGs with corresponding biocomponents, various functional biohybrids can be developed. Further, with their relatively large area, CMGs can be strongly interfaced with microscale biocomponents. This versatile bonding compatibility of the CMGs is demonstrated here by their ability to (a) attach with microscale bacterial cells, (b) tether and hybridize DNA molecules on their surface, and (c) bind with polyelectrolytes and proteins. Second, the CMGs are semiconducting nanosheets and thus undergo a highly sensitive charge-carrier modulation upon their interaction with various biological species. This is attributed to CMGs' p-type characteristics and their subnanoscale thickness, where external interactions from tiny entities can produce an extraordinary response. Furthermore, CMG devices are

* Corresponding author. E-mail: vberry@ksu.edu.

10.1021/nl802412n CCC: $40.75
Published on Web 11/05/2008

polarity-specific with a high resolution. This is shown here for (i) attachment of a single bacterium on graphene-amine (GA), which generated ~1400 conducting holes and (ii) generation of (on an average) a single quantum of hole by hybridization of approximately six complementary DNA (cDNA) strands on a graphene−DNA (G-DNA) device. Also, attachment of approximately four monomers (average) of positively charged polyallylamine hydrochloride (PAH) on the p-type graphene oxide (GO) reduced the number of holes by one quanta; while a further attachment of negatively charged polystyrene sulfonate (PSS) monolayer increased the hole density by 1.42×10^{13} cm^{-2}. We also show that the DNA tethering process on the CMGs was preferential (a) on thicker than on thinner CMGs and (b) on wrinkles than on flat surfaces of CMGs. These results show that with their modifiable chemistry and sensitive electronics, CMGs can be custom-designed and integrated with various biochemical systems to develop next-generation applications and tools such as (i) biobatteries, where electrically conducting graphene could be interfaced with *Geobacter*, a bacteria known to produce electrons on the cell wall, (ii) bioprocess analysis tools, where the cell's selective metabolism of nutrient molecules (like lysine) can be studied by measuring the H^+-potential produced on the cell wall during the ATP cycle, (iii) graphene genetic devices for pathogen identification, (iii) CMG-CMG ultrathin pn-junction solar cells, (iv) bioelectronic devices, (v) smart circuits, and (vi) molecular transistors.

In this study, the CMGs and their biohybrids were synthesized using GO or plasma-modified GA (PGA) immobilized on silica substrate. GO sheets dispersed in aqueous media were synthesized from graphite flakes (mesh 7) by the modified Hummers method.[13,25,34] This process functionalizes the surface of the GO sheets with epoxy, hydroxyl, and negatively charged carboxylic acid groups.[17] The energy dispersive X-ray spectroscopy of the samples detected the presence of oxygen. The GO was immobilized on heavily doped n-type silicon substrate with a 300 nm[35] or 1 μm thick thermally grown silica layer, patterned with predeposited or postdeposited gold electrodes (300 nm thick and 5 μm apart). The patterned substrate was first exposed to oxygen plasma (100 W, 2 mbar, 2 min) and subsequently functionalized with a monolayer of (3-aminopropyl)triethoxysilane to make the silica surface positively charged with tethered amine groups. This substrate was then immersed in the GO solution for 10 min to electrostatically deposit GO sheets on silica (Figure 1). The deposited GO sheets remained intact after thorough washing with deionized (DI) water, indicating their strong and multipoint electrostatic attachment with the substrate. Figure 1 shows the atomic force microscope (AFM) images of the GO sheets. The thickness of most GO sheets varied from 1 to 5 nm. The GO sheet scanned in Figure 1a had a thickness of ~2 nm (Figure 1a (top inset)), which corresponds to an approximately four atom thick layer of GO. This small thickness of GO confirms the effectiveness of the Hummer's method to cleave ultrathin graphene sheets and functionalizing them with negative charge.[13]

GO's surface scanned by the AFM and imaged by optical microscopy revealed the presence of sharp wrinkles (Figure 1a bottom inset), which were 6−8 nm in height, ~30−50 nm in width, and several micrometers long (Figure 1a, top right inset). The lack of directional preference of these wrinkles indicated that they were entropically formed.[36,37] Further, these long wrinkles were observed in a greater quantity on larger GO sheets (>20 μm) than on the smaller ones (<5−10 μm) and more at the center than on the edges. These results indicate that the wrinkle formation was a result of multiple-point electrostatic anchoring of GO sheets, producing wrinkles in the middle. The AFM and the optical microscopy images also showed the presence of folds and multilevel layering of sheets (Figure 1b). In Figure 1b we have marked the regions of different relative thicknesses (not the number of layers) of GO sheets, thus illustrating the multilevel structure of GO. PGA was synthesized either by exposing the graphite flakes to ammonia (or nitrogen plasma) followed by exfoliation via sonication in water or by exposing the GO sheets immobilized on a silica substrate to hydrogen plasma followed by ammonia (or nitrogen) plasma.

The GO sheets immobilized on silica were used as templates to selectively and covalently tether single-stranded DNA to build the G-DNA hybrid. The GO−silica substrate was immersed in a solution mixture of 5′-pentamine-terminated DNA with 20 bases (amine-AAC TGC CAG CCT AAG TCC AA) and *O*-(7-azabenzotriazole-1-yl)-*N*,*N*,*N*,*N*′-tetramethyluronium hexafluorophosphate (HATU) (an amide-coupling reagent), at room temperature for 8 h in an incubator. Since this DNA's terminal amine group bonds covalently with the carboxylic group on GO and not with the amine groups on silica, the reaction resulted in selective DNA tethering on the GO sheets. The physically adsorbed DNA molecules were removed by a 1% sodium dodecyl sulfate (SDS) wash for 30 min. The tethering of this target DNA was verified by hybridizing it with a fluorescent cDNA probe (dye-TTG GAC TTA GGC TGG CAG TT) terminated with 3′-rhodamine green dye (522 nm emission). The hybridization process was conducted by placing a drop of the probe DNA on the G-DNA substrate followed by incubation at room temperature for 4 h. The nonspecifically bound DNA was removed by a 30 min wash with 1% SDS solution.

Under a confocal microscope, fluorescence at 522 nm confirmed the successful synthesis of G-DNA hybrids (Figure 2, panels a and b) with DNA tethered on its surface. The confocal images (Figure 2, panels a and b) further show that the DNA preferentially tethers on thicker layers (including folds) and on wrinkles of GO as depicted by a higher fluorescence intensity in these regions. This was verified by the *z*-stack images from the confocal microscope. The insets of panels a and b of Figure 2 show the optical image of the corresponding G-DNA. Since the dye molecules are at least 7.2 nm (20 base DNA + seven-carbon chain) from the GA surface, the observed florescence contrast is not due to quenching,[38] electromagnetic enhancement,[38] or background overlapping. The bottom-left inset of Figure 2a shows the effect of GO thickness on the relative fluorescence intensity

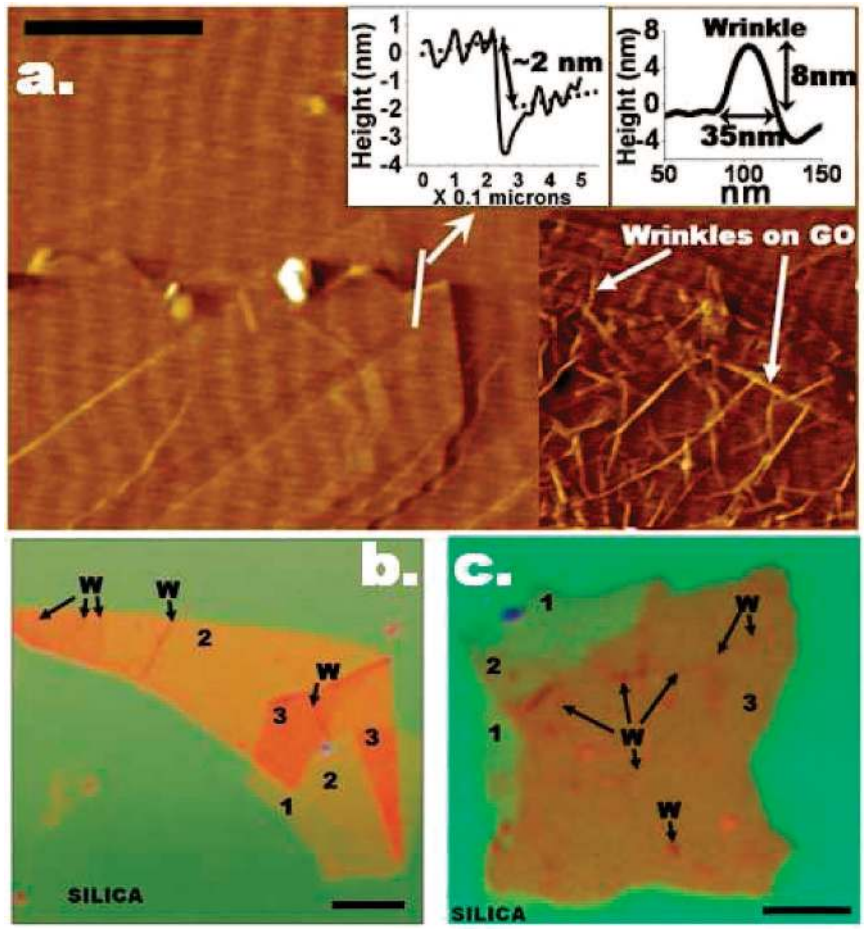

Figure 1. (a) AFM image (3.1 × 1.9 μm^2) of GO sheets deposited on silica substrate. Top left inset shows the thickness of a GO sheet to be ~2 nm (approximately four atoms thick). Bottom inset shows an AFM image showing the several wrinkles on the GO's surface. Top right inset shows the height and width of a typical wrinkle on GO. (b, c) Optical microscope images (inverted colors) of GO on 300 nm silica substrate are shown. Here 1, 2, and 3 represent the relative thickness of GO sheets and W represents the wrinkles. Bar size = 5 μm.

and thus the DNA density. This contrast in DNA density can be attributed to dissimilar surface potential at different layer thicknesses caused by a difference in the magnitude of intrinsic screening of the interfacial traps or defects on silica surface.[39] This causes a higher surface potential on thicker surfaces which in turn leads to more favorable DNA binding. This variable surface potential for different thicknesses has been shown for pristine graphene.[39] Similarly, the higher DNA density on the surface wrinkles can be attributed to the local field enhancement at the sharp edges of the wrinkles.[40,41] Furthermore, the absence of enhanced fluorescence at the G-DNA edges indicates that, for a particular GO thickness, the carboxylic acid groups are uniformly distributed[42] on GO surface with no selectivity for the edge, contrary to the earlier report.[17,43] Similar uniform functionalization of carboxylic group has been reported for carbon nanotubes.[44,45] Two control experiments by omitting (a) the probe-DNA attachment step and (b) the target-DNA attachment step showed no fluorescence under confocal microscope, thus validating the results (Figure 2, panels c and d). Omitting HATU-reagent from the process led to a sharp decrease in the florescence intensity on G-DNA, indicating that the presence of HATU is crucial for stronger DNA binding.

The CMG/bacteria hybrid was built by selectively assembling microscale negatively charged bacterial cells on positively charged GA scaffolds synthesized by aminization of the immobilized GO sheets on silica substrate. A high selectivity of bacterial assembly was achieved by making the silica substrate hydrophobic by treating it with valeric acid and HATU. This process tethers a five-carbon-chain molecule on silica. The GO to GA conversion was achieved by immersing the substrate in a solution mixture of ethylenediamine (EDA) and HATU for 8 h at room temperature. In this reaction, one amine group of the EDA molecule bonds with the carboxylic groups on GO, while the other amine group remains unreacted on the surface, thus producing positively charged GA sheets surrounded by hydrophobic silica substrate (Figure 3a, bottom inset).

The Gram-positive *Bacillus cereus* cells were employed to fabricate the bacteria/CMG ensembles. These cells possess a highly negatively charged surface due to the polyteichoic acid molecules densely tethered on their cell wall.[3,46] The *Bacillus cereus* cells were first cultured in LB media in an incubator shaker at 37 °C for 14 h (log phase). The cells were subsequently washed five times by centrifuging (2000 rpm (400*g*), 5 min) and resuspending in DI water. With a strong cell wall, these bacterial cells do not undergo lysis in

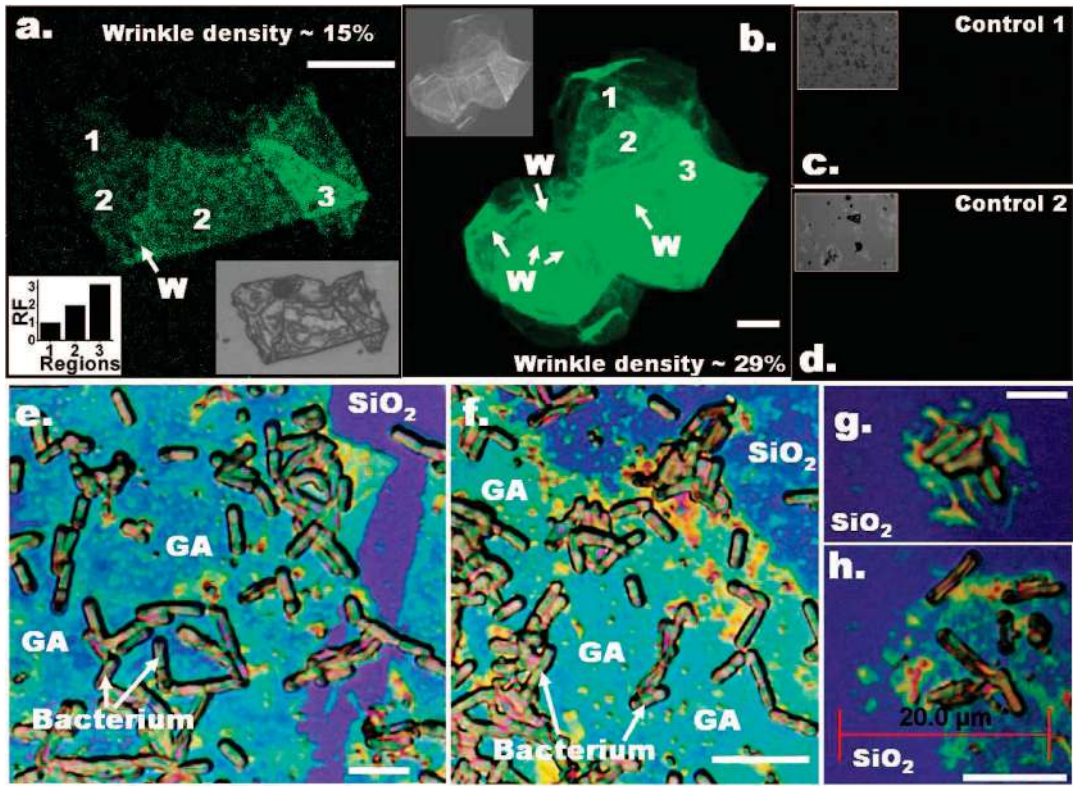

Figure 2. (a, b) Confocal images showing florescent-labeled probe-DNA hybridized on the target-DNA covalently attached on GO sheets. The folds and wrinkles on G-DNA sheets are easily visible via florescence-contrast. 1, 2, and 3 represent the relative thickness of G-DNA sheets and W represents wrinkles (confirmed by *z*-stack). The bottom-right inset of (a) and the top inset of (b) show the optical images of the corresponding G-DNA sheets; while the bottom-left inset of (a) shows the relative intensities in regions 1, 2, and 3 of (a). (c) and (d) Control-confocal images for no probe-DNA and no target-DNA, respectively. (e) and (f) Microscope images showing selective attachment of bacterial cells on GA. (g) and (h) Selective deposition of bacteria on smaller GA sheets. Bar size = 10 μm.

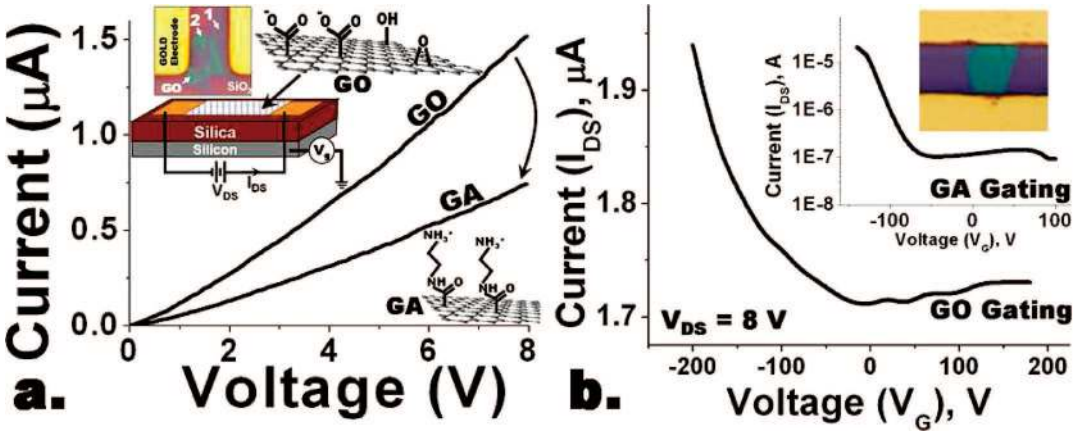

Figure 3. (a) Current−voltage behavior of the GO and GA devices. GA devices always show lower conductivity than their parent GO devices. The increase in conductivity with voltage is slightly nonlinear for both GO and GA devices. The insets show the device with GO/GA between gold electrodes and a schematic of the GO and GA's chemical structure. (b) Electrical gating of GO and GA shows that they are p-type semiconductors. The top inset shows the postdeposited gold electrodes on a GO sheet.

DI water.[2,3,46] The previously prepared GA substrate was immediately immersed in the purified bacterial suspension for 5 min, followed by washing with DI water and drying in a jet of dry nitrogen. This led to electrostatic deposition of the bacterial cells on GA as shown in Figure 2, panels e and f. Further, the hydrophobicity of silica surface enhanced the selectivity of deposition (Figure 2, panels g and h) on GA. This indicates that the adhesion of bacteria on GA is not governed by the (sticky) surface protein and is purely electrostatic. There were also no signs of bacterial lysis, with the cells retaining their integrity on GA. Further, to determine whether the bacteria deposited on GA were live, a LIVE/DEAD test was conducted by staining the bacteria on the samples with Syto-9 and PI for 1 min. Under confocal microscopy, the bacteria which were alive appear green in color (syto-9 staining) and the ones which were dead appear red in color (PI staining). It was confirmed that most of the cells on GA were alive (Figure 4a, inset 3) after their

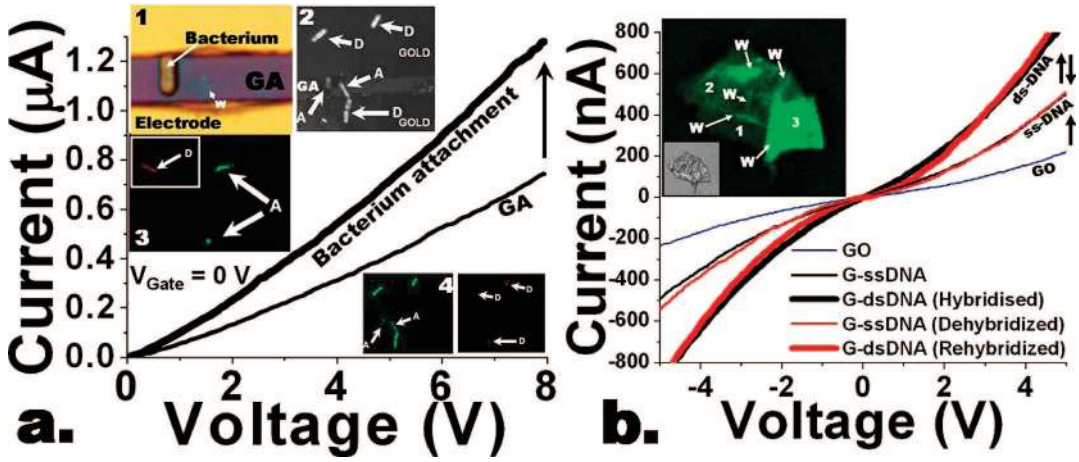

Figure 4. (a) The conductivity of the p-type GA device increases upon attachment of a single bacterial cell on the surface of GA (inset 1). LIVE/DEAD confocal microscopy test on the bacteria deposited on GA confirmed that most of the bacteria were alive after the electrostatic deposition (inset 3). *A* = alive and *D* = dead. The LIVE/DEAD test conducted immediately after the electrical measurements on the GA−gold−bacteria device (inset 2 and inset 4) showed that the bacterial cells on GA atop silica remain alive, while the bacteria deposited on the GA atop gold electrodes die after electrical measurements (inset 4 (right)). (b) DNA transistor: ss-DNA tethering on GO increases the conductivity of the device. Successive hybridization and dehybridization of DNA on the G-DNA device results in completely reversible increase and restoration of conductivity. Inset shows a G-DNA(ds) sheet with wrinkles and folds clearly visible.

deposition, an observation similar to an earlier report.[3] The bacteria, however, die after about 4 h (see Supporting Information). The deposition of bacteria of all sizes (or life cycle stages) indicates that their negative charge polarity is not size dependent. No preferential deposition of these relatively large sized (~4−5 μm) bacterial cells was observed with respect to the wrinkles or the edges of the GA sheets, indicating uniformity of the charge on GA at a larger scale. The deposited bacteria did not detach from the surface when washed with DI water at room temperature, thus illustrating the strong binding between bacteria and the CMG. However, rigorous washing with DI water at 80 °C did cause the bacteria to peel off. Further, to increase the affinity and specificity of bacterial attachment on CMG, GO was tethered with concanavalin, a biomolecule with highly specific affinity to the teichoic acid on the peptidoglycan membrane of the bacterial cell wall. The bacterial attachment density on this CMG-concanavalin conjugate was found to be extremely high and very specific. Confocal microscopy was used to confirm the tethering of the concanavalin-FITC conjugate on GO and to confirm the subsequent attachment density of the bacterial cells (Supporting Information).

Electrical measurements of GO and GA sheets immobilized on silica substrate with predeposited or postdeposited gold electrodes (Figure 3 top inset) and silicon as backgate were conducted to determine the semiconductor characteristics of the CMGs. Here, the GA devices were produced by direct aminization of the GO devices (as explained above). Both GO and GA exhibited a slightly nonlinear current−voltage behavior (Figure 3a) in dry nitrogen atmosphere, with the GA device always having a lower conductivity than the parent GO devices (Figure 3a). Both the GO and GA devices were p-type semiconductors (Figure 3b). For the device shown in Figure 3a, top inset, the hole mobilities for GO and GA were 0.0297 ± 0.0017 (cm^2/V)/s and 5.882 ± 0.098 (cm^2/V)/s, respectively, while the electron mobilities were ~0.00198 ± 0.0002 and 0.00747 ± 0.00178 (cm^2/V)/s, respectively. These carrier mobilities ($\mu_{Carrier}$) were calculated from the following expression

$$\mu_{Carrier} = (\Delta I_{DS}/\Delta V_G)/(C_G(l/w)V_{DS}) \quad (1)$$

Here, ΔI_{DS} and V_{DS} are the source−drain current and voltage, C_G is the capacitance of the silica gate, and l and w are the length and width of the CMG sheets between electrodes. The higher hole mobility of GA can be attributed to the relatively large distance between the charged amine group and the graphene base as compared to the distance between carboxylic group and the graphene base for GO. The density of holes in GA is ~2100-fold less than that in GO. Further, the hole mobility of GA was always higher than that of the parent GO device and increases with increasing aminization time scale. Devices with postdeposited gold electrodes on GO produced similar results (Figure 3b, top inset) (see Supporting Information).

Bacterial attachment on a GA device was tested for CMG's microbial interfacing sensitivity and resolution. The GA device exhibited a sharp 42% increase in conductivity upon attachment of a single bacterial cell on GA (method explained above) (Figure 4a). This can be attributed to the p-type characteristic of GA, where the attachment of a negatively charged species such as bacteria, is equivalent to a negative potential gating which increases the hole density and thus the conductivity of GA. The hole density increase due to the bacterium attachment (Figure 4a, top inset) was calculated to be 3.53 × 10^{10} cm^{-2} ($R_1|_{GA}$ = 10.85 ± 0.51 MΩ, $R_2|_{Bacteria}$ = 6.3 ± 0.4 MΩ). This corresponds to a generation of ~1400 holes per bacterium in GA. The change in hole density (Δq) was calculated by the expression

$$\Delta q = (R_2^{-1} - R_1^{-1})/((l/w)\mu_p) \quad (2)$$

Here R_2 and R_1 are the final and initial resistances of the device. Since all the measurements were conducted in a dry nitrogen atmosphere, with bacteria not touching both electrodes simultaneously, there was no ionic conductivity from

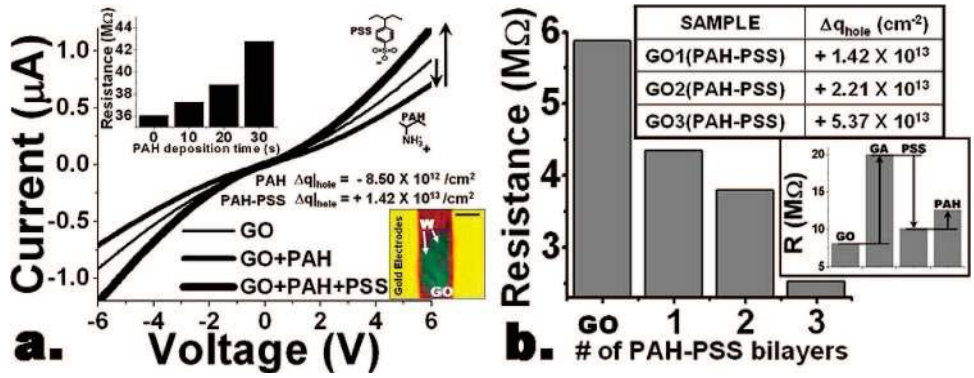

Figure 5. (a) The conductivity and the hole density of GO decreases and increases with attachment of PAH and PSS, respectively. Top inset: Increasing the areal density of attached PAH on GO, by increasing deposition time, leads to increase in gating of GO between the electrodes (bottom inset), reducing its conductivity. Bottom inset's bar size = 4 μm. (b) Resistance reduces (negative potential gating) with increase in the number of PAH−PSS bilayer. The top inset shows the change in the hole density. The bottom inset shows the change in resistance of a GO device functionalized to a GA device followed by attachment of a PSS monolayer and subsequent attachment of a PAH monolayer.

bacteria. Also application of electric field for long durations did not change the conductivity as expected for ionic conductivity. This further shows that the chemical gating on GA was partially a result of the compensation of the positive charge of the amine groups on GA by the negative charge of the polyteichoic acid molecules on the bacterial surface. Further, the LIVE/DEAD test on a bacterial device after electrical measurements showed that the bacteria on GA atop silica remain alive immediately after an electrical measurement; however the cells deposited on GA atop gold electrodes died (Figure 4a, inset). A typical *IV* electrical measurement comprises of an application of an average of ~4 V (dc) for a net time of 1.6 s (total time of ~10 min). The electrical measurements and the nitrogen atmosphere did not have any visible effect on the integrity of the bacterium's structure as against the CNT network devices.[12] These results show a proof-of-concept of a highly sensitive graphene-based biodiagnostic tool with single-bacterium resolution. Further, some advantages of the CMG/bacteria device over the optical-detection methods are that (a) the CMG/bacteria device does not require the lengthy process of florescent[47] or magnetic[48] labeling of bacteria required for some optical methods, (b) it does not require high computation power for image analysis[47,49] necessary for most optical methods, (c) the optical methods require expensive optics such as CCDs, lasers, etc.,[47−50] and (d) to attract the bacteria most optical methods are coupled with external ultrasonic standing wave generators.[50] A CMG/bacteria device would not require external instruments for bacterial trapping, which can be achieved by electropheresis[51] by application of a small ac voltage on the device electrodes. Further, as shown earlier, high specificity can be achieved by the CMGs devices by tethering them with biomolecules, like concanavalin, with high affinity to the bacterial cell wall.

Electrical characterization of the G-DNA hybrids was conducted to examine CMG's viability and sensitivity as a biomolecular transistor. First, selective tethering of the single-stranded DNA on GO to form G-DNA was carried out (method explained earlier). This led to a 128% increase in the conductivity, partially attributed to the attachment of the negatively charged DNA on the p-type GO (Figure 4b). Subsequently, hybridization with cDNA was conducted on the G-DNA device (explained earlier). This led to a 71% increase in conductivity ($R_1|_{DNA} = 9.86 \pm 0.24$ MΩ; $R_2|_{dsDNA} = 5.77 \pm 0.17$ MΩ) (Figure 4 b). The robustness of this device was tested by dehybridizing the cDNA from G-DNA (see Supporting Information), which resulted in the restoration of G-DNA's original conductivity (Figure 4b). Further, multiple hybridization−dehybridization runs showed consistent increase and restoration of the conductivity. The increase in the hole density upon DNA hybridization was $+5.61 \times 10^{12}$ cm^{-2} (eq 2), which in turn implies that one quanta of hole is generated or removed by hybridization or dehybridization of approximately six DNA molecules (see Supporting Information). This figure is calculated assuming a carboxylic acid density on GO of 1.623×10^{14} cm^{-2},[52] a DNA attachment efficiency of 25%, and a hybridization efficiency of 90%.[53] The generation of holes is attributed to the negative-charge molecular gating from the phosphate ions of the complementary DNA. The change in conductivity due to hybridization/dehybridization varied from 60% to 200% for different G-DNA samples. Immersing the G-DNA device in a solution of non-complementary DNA did not change the conductivity. Even though the DNA hybridization/dehybridization measurements were made in dry nitrogen conditions, they were effective in producing the negative-charge-gating. These results further elucidate the high sensitivity of CMG-nanostructures which function effectively as a label-free DNA detector and a molecular transistor.

To examine the CMG molecular transistor's specificity to polarity, a positively charged PAH monolayer[54] (70000 Da; 2.5 mg/mL; 10 min deposition) was deposited on GO. This led to an increase in its resistance corresponding to a decrease in hole density ($R_1|_{GO} = 5.88 \pm 0.3$ MΩ, $R_2|_{GO\text{-}PAH} = 7.47 \pm 0.31$ MΩ, $\Delta q_h = -8.5 \times 10^{12}$ cm^{-2}) (Figure 5a). It was calculated (eq 3) that on an average 1 PAH monomer is electrostatically attached on 3 nm^2 of GO surface (see Supporting Information)

$$n = (4\pi(h^2/dl_P)_{PAH}W^2\Delta I_{DS})/(e\mu V_{DS}) \quad (3)$$

Here h, d, and l_P are the height, the width, and the length of a PAH monomer. This further implies that attachment of approximately four PAH monomers reduces a single quantum of hole (see Supporting Information). Furthermore, the PAH attachment (Figure 5a inset (top)) showed a monotonous decrease in conductivity with an increase in duration of attachment, reaching saturation in ~3 min. This is attributed to a continuous decrease in number of holes as more and more PAH deposits on GO. Attaching a monolayer of negatively charged PSS (70000 Da, 2.5 mg/mL, 10 min) on the GO−PAH device increased the conductivity corresponding to an increase in hole density, equivalent to a negative-potential gating (Figure 5a) ($R_1|_{GO\text{-}PAH} = 7.47 \pm 0.31$ MΩ; $R_2|_{GO\text{-}PAH\text{-}PSS} = 4.41 \pm 0.43$ MΩ, $\Delta q_h = +1.42 \times 10^{13}$ cm^{-2}). This shows that the GO device undergoes a polarity specific gating with increase or decrease in conductivity upon attachment of negatively or positively charged species, respectively. This further shows that the CMG gating is sensitive to molecular adsorption at distances more than that of a single polyelectrolyte monolayer. Indeed attachment of two more layers of PAH and PSS each (six monolayers with a thickness of ~13.6 nm[54]) led to continued gating of the underlying GO (Figure 5b, top inset). The nonunidirectional (increase and decrease) change in conductivity observed by differently charged molecules negates the phenomenon originating from a change in ionic conductivity, contact resistance, or thermal effects, where the response is expected to be unidirectional. GA devices also show similar results for molecular attachment. Electrostatic attachment of PSS followed by PAH on a GA device led to an increase and decrease in conductance, respectively ($R_1|_{GO} = 8.11 \pm 0.5$ MΩ; $R_2|_{GA} = 20.0 \pm 0.5$ MΩ; $R_3|_{GA\text{-}PSS} = 10.1 \pm 0.6$ MΩ; $R_4|_{GO\text{-}PSS\text{-}PAH} = 12.6 \pm 0.51$ MΩ). These results show that (a) response direction of CMG transistors is polarity specific, (b) CMGs can be designed to respond to any polarity, and (c) CMG gating is sensitive over several multilayers of adsorption. PGA synthesized by nitrogen−helium plasma treatment of graphite also showed a p-type nature and polyelectrolyte attachment sensitivity similar to GA (see Supporting Information).

A study of a protein transistor was conducted to establish the relationship between device sensitivity and fabrication process. GA produced from extensive aminization of parent GO underwent a high 30-fold increase in resistance ($R_1|_{GO} = 26.67 \pm 0.9$ MΩ; $R_2|_{GA} = 800.1 \pm 2$ MΩ). Electrostatic adsorption of a mixture of negatively charged bacterial DNA and proteins extracted from *Bacillus cereus* (see Supporting Information) on this GA device led to a sharp 2 orders of magnitude decrease in resistance ($R_1|_{GA} = 800.1 \pm 2$ MΩ; $R_2|_{GA\text{-}Bacteria\text{-}proteins} = 5.34 \pm 0.2$ MΩ, $\Delta q_h = +1.81 \times 10^{11}$ hole/cm^2) (Figure 6). This extremely high sensitivity of GA is attributed to the extensive aminization of GO to form GA, where the EDA bonding on GO partially acts as a gating process for the base graphene-carbonitrile (GC) sheets (Figure 6, inset). Generally, the GA devices which underwent a larger decrease in conductivity after aminization, or a higher positive gating (partial) of the GC base, have higher sensitivity to negative species attachment. Since the aminization process can be controlled by deposition time, it provides the ability to tune CMG's sensitivity.

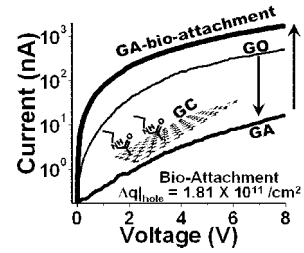

Figure 6. GA produced from extensive aminization of GO, via covalent attachment of the ethylenediamine, led to 30-fold reduction in conductivity. Further electrostatic attachment of negatively charged bacterial protein and DNA on the GA device led to 100-fold increase in conduction due to negative charge gating. The inset shows a CMG of graphene carbonitrile (GC).

In conclusion, we have demonstrated the viability of CMGs as sensitive building blocks for bioelectronics at both microbial and molecular levels. Specifically, we demonstrated (i) a single bacterium resolution interfacial device, (ii) a label-free, reversible DNA detector, and (iii) a polarity-specific molecular transistor for protein/DNA adsorption. We also illustrated the ability to control the sensitivity, polarity specificity, and the extent of gating of the CMGs. This study will potentially motivate the development of a tool kit of graphene derivatives to apply them in building next-generation systems and devices such as biodriven electronic devices, biodetection tools, biobatteries, smart electrochemical circuitry, and molecular electronic systems.

Acknowledgment. V.B. would like to thank Kansas State University for the start-up funds. We would like to thank Jose Armesto, Ashvin Nagaraja, and Kabeer Jasuja for help with plasma treatment of graphite, bacterial samples, and electrical measurements, respectively.

Supporting Information Available: Fabrication and electrical properties of GO, GA, bacteria/GA ensemble, G-DNA, PGA and protein-GA devices, more examples of CMG sheets with wrinkles, folds, and multilayers, and calculations for DNA attachment and PAH attachment.This material is available free of charge via the Internet at http://pubs.acs.org.

References

(1) Liao, H. W.; Nehl, C. L.; Hafner, J. H. Biomedical applications of plasmon resonant metal nanoparticles. *Nanomedicine* **2006**, *1*, 201–208.
(2) Berry, V.; Rangaswamy, S.; Saraf, R. F. Highly selective, electrically conductive monolayer of nanoparticles on live bacteria. *Nano Lett.* **2004**, *4*, 939–942.
(3) Berry, V.; Saraf, R. F. Self-assembly of nanoparticles on live bacterium: An avenue to fabricate electronic devices. *Angew. Chem., Int. Ed.* **2005**, *44*, 6668–6673.
(4) Cai, H.; Cao, X. N.; Jiang, Y.; He, P. G.; Fang, Y. Z. Carbon nanotube-enhanced electrochemical DNA biosensor for DNA hybridization detection. *Anal. Bioanal. Chem.* **2003**, *375*, 287–293.
(5) Cui, Y.; Wei, Q. Q.; Park, H. K.; Lieber, C. M. Nanowire nanosensors for highly sensitive and selective detection of biological and chemical species. *Science* **2001**, *293*, 1289–1292.
(6) Patolsky, F.; Zheng, G. F.; Lieber, C. M. Nanowire-based biosensors. *Anal. Chem.* **2006**, *78*, 4260–4269.

(7) Cai, H.; Xu, C.; He, P. G.; Fang, Y. Z. Colloid Au-enhanced DNA immobilization for the electrochemical detection of sequence-specific DNA. *J. Electroanal. Chem.* **2001**, *510*, 78–85.
(8) Le, J. D.; Pinto, Y.; Seeman, N. C.; Musier-Forsyth, K.; Taton, T. A.; Kiehl, R. A. DNA-templated self-assembly of metallic nanocomponent arrays on a surface. *Nano Lett.* **2004**, *4*, 2343–2347.
(9) Cai, H.; Xu, C.; He, P. G.; Fang, Y. Z. Colloid Au-enhanced DNA immobilization for the electrochemical detection of sequence-specific DNA. *J. Electroanal. Chem.* **2001**, *510*, 78–85.
(10) Cui, Y.; Wei, Q. Q.; Park, H. K.; Lieber, C. M. Nanowire nanosensors for highly sensitive and selective detection of biological and chemical species. *Science* **2001**, *293*, 1289–1292.
(11) Patolsky, F.; Zheng, G. F.; Lieber, C. M. Nanowire-based biosensors. *Anal. Chem.* **2006**, *78*, 4260–4269.
(12) So, H. M.; Park, D.-W.; Jeon, E.-K.; Kim, Y.-H.; Lee, C.-K.; Choi, S. Y.; Kim, S. C.; Chang, H.; Lee, J.-O. Detection and titer estimation of *Escherichia coli* using aptamer-functionalized single-walled carbon-nanotube field-effect transistors. *Small* **2008**, *4*, 197–201.
(13) Gilje, S.; Han, S.; Wang, M.; Wang, K. L.; Kaner, R. B. A chemical route to graphene for device applications. *Nano Lett.* **2007**, *7*, 3394–3398.
(14) Stankovich, S.; Dikin, D. A.; Dommett, G. H. B.; Kohlhass, K. M.; Zimney, E. J.; Stach, E. A.; Piner, R. D.; Nguyen, S. T.; Ruoff, R. S. Graphene-based composite materials. *Nature* **2006**, *442*, 282–286.
(15) Hod, O.; Peralta, J. E.; Scuseria, G. E. Edge effects in finite elongated graphene nanoribbons. *Phys. Rev. B* **2007**, *76*, 233401.
(16) Gomez-Navarro, C.; Weitz, R. T.; Bittner, A. M.; Scolari, M.; Mews, A.; Burghard, M.; Kern, K. Electronic transport properties of individual chemically reduced graphene oxide sheets. *Nano Lett.* **2007**, *7*, 3499–3503.
(17) Park, S.; Lee, K.-S.; Bozoklu, G.; Cai, W.; Nguyen, S. T.; Ruoff, R. S. Graphene oxide papers modified by divalent ions - Enhancing mechanical properties via chemical cross-linking. *ACS Nano* **2008**, *2*, 572–578.
(18) Yan, Q. M.; Huang, B.; Yu, J.; Zheng, F.; Zang, J.; Wu, J.; Gu, B.-L.; Liu, F.; Duan, W. Intrinsic current-voltage characteristics of graphene nanoribbon transistors and effect of edge doping. *Nano Lett.* **2007**, *7*, 1469–1473.
(19) Obradovic, B.; et al. Analysis of graphene nanoribbons as a channel material for field-effect transistors. *Appl. Phys. Lett.* **2006**, 88.
(20) Barone, V.; Hod, O.; Scuseria, G. E. Electronic structure and stability of semiconducting graphene nanoribbons. *Nano Lett.* **2006**, *6*, 2748–2754.
(21) Novoselov, K. S.; Geim, A. K.; Morozov, S. V.; Jiang, D.; Zhang, Y.; Dubonos, S. V.; Grigorieva, I. V.; Firsov, A. A. Electric field effect in atomically thin carbon films. *Science* **2004**, *306*, 666–669.
(22) Novoselov, K. S.; Geim, A. K.; Morozov, S. V.; Jiang, D.; Katsnelson, M. I.; Grigorieva, I. V.; Dubonos, S. V.; Firsov, A. A. Two-dimensional gas of massless Dirac fermions in graphene. *Nature* **2005**, *438*, 197–200.
(23) Berger, C.; Song, Z.; Li, X.; Wu, X.; Brown, N.; Naud, C.; Mayou, D.; Li, T.; Hass, J.; Marchenkov, A. N.; Conrad, E. H.; First, P. N.; de Heer, W. A. Electronic confinement and coherence in patterned epitaxial graphene. *Science* **2006**, *312*, 1191–1196.
(24) Zhou, S. Y.; Gweon, G.-H.; Graf, J.; Fedorov, A. V.; Spararu, C. D.; Diehl, R. D.; Kopelevich, Y.; Lee, D.-H.; Louie, S. G.; Lanzara, A. First direct observation of Dirac fermions in graphite. *Nat. Phys.* **2006**, *2*, 595–599.
(25) Geim, A. K.; Novoselov, K. S. The rise of graphene. *Nat. Mater.* **2007**, *6*, 183–191.
(26) Schedin, F.; et al. Detection of individual gas molecules adsorbed on graphene. *Nat. Mater.* **2007**, *6*, 652–655.
(27) Jian-Hao Chen et al. Printed Graphene Circuits. *Adv. Mater.* Early View, (2007).
(28) Wu, Y. Q. Top-gated graphene field-effect-transistors formed by decomposition of SiC. *Appl. Phys. Lett.* **2008**, *92*, 092102.
(29) Liu, Q.; Liu, Z.; Zhang, X.; Zhang, N.; Yang, L.; Yin, S.; Chen, Y. Organic photovoltaic cells based on an acceptor of soluble graphene. *Appl. Phys. Lett.* **2008**, *92*, 223303.
(30) Wang, X. Transparent carbon films as electrodes in organic solar cells. *Angew. Chem., Int. Ed.* **2008**, *47*, 2990–2992.
(31) Becerril, H. A.; Mao, J.; Liu, Z.; Stoltenberg, R. M.; Bao, Z.; Chen, Y. Evaluation of solution-processed reduced graphene oxide films as transparent conductors. *ACS Nano* **2008**, *2*, 463–470.
(32) Wang, X.; Zhi, L. J.; Mullen, K. Transparent, conductive graphene electrodes for dye-sensitized solar cells. *Nano Lett.* **2008**, *8*, 323–327.
(33) Blake, P.; Brimicombe, P. D.; Nair, R. R.; Booth, T. J.; Jiang, D.; Schedin, F.; Ponomarenko, L. A.; Morozov, S. V.; Gleeson, H. F.; Hill, E. W.; Geim, A. K.; Novoselov, K. S. Graphene-Based Liquid Crystal Device. *Nano Lett.* **2008**, *8*, 1704–1708.
(34) Hummers, W. S.; Offeman, R. E. Preparation of Graphitic Oxide. *J. Am. Chem. Soc.* **1958**, *80*, 1339.
(35) Blake, P.; Hill, E. W.; Castro Neto, A. H.; Novoselov, K. S.; Jiang, D.; Yang, R.; Booth, T. J.; Geim, A. K. Making graphene visible. *Appl. Phys. Lett.* **2007**, *91*, 063124.
(36) Meyer, J. C.; Geim, A. K.; Katsnelson, M. I.; Novoselov, K. S.; Booth, T. J.; Roth, S. The structure of suspended graphene sheets. *Nature* **2007**, *446*, 60–63.
(37) Meyer, J. C.; Geim, A. K.; Katsnelson, M. I.; Novoselov, K. S.; Obergfell, D.; Roth, S.; Girit, C.; Zettl, A. On the roughness of single- and bi-layer graphene membranes. *Solid State Commun.* **2007**, *143*, 101–109.
(38) Stoermer, R. L.; Keating, C. D. Distance-dependent emission from dye-labeled oligonucleotides on striped Au/Ag nanowires: Effect of secondary structure and hybridization efficiency. *J. Am. Chem. Soc.* **2006**, *128*, 13243–13254.
(39) Datta, S. S., Strachan, D. R., Mele, E. J., Johnson, A. T. C. Surface Potentials and Layer Charge Distributions in Few-Layer Graphene Films. *Nano Lett.*, DOI: 10.1021/nl8009044.
(40) Kokkorakis, G. C.; Xanthakis, J. P. Local electric field and enhancement factor around nanographitic structures embedded in amorphous carbon. *Surf. Interface Anal.* **2007**, *39*, 135–138.
(41) Ferris, K. F.; Risser, S. M. Surface Defect Enhancement of Local Electric-Fields in Dielectric Media. *Chem. Phys. Lett.* **1995**, *234*, 359–366.
(42) Mermoux, M.; Chabre, Y.; Rousseau, A. FTIR and C-13 NMR-Study of Graphite Oxide. *Carbon* **1991**, *29*, 469–474.
(43) He, H. Y.; Riedl, T.; Lerf, A.; Klinowski, J. Solid-state NMR studies of the structure of graphite oxide. *J. Phys. Chem.* **1996**, *100*, 19954–19958.
(44) Holzinger, M.; Vostrowsky, O.; Hirsch, A.; Hennrich, F.; Kappes, M.; Weiss, R.; Jellen, F. Sidewall functionalization of carbon nanotubes. *Angew. Chem., Int. Ed.* **2001**, *40*, 4002-+
(45) Jiang, K. Y.; Schradler, L. S.; Siegel, R. W.; Zhang, X.; Terrones, M. Protein immobilization on carbon nanotubes via a two-step process of diimide-activated amidation. *J. Mater. Chem.* **2004**, *14*, 37–39.
(46) Berry, V.; Gole, A.; Kundu, S.; Murphy, C. J.; Saraf, R. F. Deposition of CTAB-terminated nanorods on bacteria to form highly conducting hybrid systems. *J. Am. Chem. Soc.* **2005**, *127*, 17600–17601.
(47) Matsunaga, T.; Nakayama, H.; Okochi, M.; Takeyama, H. Fluorescent detection of cyanobacterial DNA using bacterial magnetic particles on a MAG-microarray. *Biotechnol. Bioeng.* **2001**, *73*, 400–405.
(48) Baldrich, E.; Munoz, F. X. Enzyme shadowing: using antibody-enzyme dually-labeled magnetic particles for fast bacterial detection. *Analyst* **2008**, *133*, 1009–1012.
(49) Bloem, J.; Veninga, M.; Shepherd, J. Fully-Automatic Determination of Soil Bacterium Numbers, Cell Volumes, and Frequencies of Dividing Cells by Confocal Laser-Scanning Microscopy and Image-Analysis. *Appl. Environ. Microbiol.* **1995**, *61*, 926–936.
(50) Zourob, M.; Hawkes, J. J.; Coakley, W. T.; Treves Brown, B. J.; Fielden, P. R.; McDonnell, M. B.; Goddard, N. J. Optical leaky waveguide sensor for detection of bacteria with ultrasound attractor force. *Anal. Chem.* **2005**, *77*, 6163–6168.
(51) Beck, J. D.; Shang, L.; Marcus, M. S.; Hamers, R. J. Manipulation and real-time electrical detection of individual bacterial cells at electrode junctions: A model for assembly of nanoscale biosystems. *Nano Lett.* **2005**, *5*, 777–781.
(52) Stankovich, S.; Dikin, D. A.; Piner, R. D.; Kohlhaas, K. A.; Kleinhammes, A.; Jia, Y.; Wu, Y.; Nguyen, S. T.; Ruoff, R. S. Synthesis of graphene-based nanosheets via chemical reduction of exfoliated graphite oxide. *Carbon* **2007**, *45*, 1558–1565.
(53) Peterson, A. W.; Heaton, R. J.; Georgiadis, R. M. The effect of surface probe density on DNA hybridization. *Nucleic Acids Res.* **2001**, *29*, 5163–5168.
(54) Decher, G. Fuzzy nanoassemblies: Toward layered polymeric multicomposites. *Science* **1997**, *277*, 1232–1237.

NL802412N